Stochastic modeling of molecular charge transport networks

Björn Baumeier,[1,*] Ole Stenzel,[2] Carl Poelking,[1] Denis Andrienko,[1] and Volker Schmidt[2]

[1]*Max Planck Institute for Polymer Research, Ackermannweg 10, 55128 Mainz, Germany*
[2]*Institute of Stochastics, Ulm University, Helmholtzstrasse 18, 89069 Ulm, Germany*

We develop a stochastic network model for charge transport simulations in amorphous organic semiconductors, which generalizes the correlated Gaussian disorder model to realistic morphologies, charge transfer rates, and site energies. The network model includes an iterative dominance-competition model for positioning vertices (hopping sites) in space, distance-dependent distributions for the vertex connectivity and electronic coupling elements, and a moving-average procedure for assigning spatially correlated site energies. The field dependence of the hole mobility of the amorphous organic semiconductor, tris-(8-hydroxyquinoline)aluminum, which was calculated using the stochastic network model, showed good quantitative agreement with the prediction based on a microscopic approach.

PACS number(s): 72.80.Le, 71.23.−k, 72.80.Ph, 73.63.Bd

I. INTRODUCTION

The design of materials for organic electronic devices is driven by optimization of charge and energy transfer processes within them.[1,2] These processes are strongly influenced by an interplay of effects on various length and time scales, ranging from macroscopic morphological order to quantum phenomena at an atomic resolution. Theory and simulations have substantially contributed to our understanding of these processes in amorphous organic semiconductors; in particular (extended, correlated) Gaussian disorder models (GDM) have been successful in rationalizing the influence of finite carrier concentration, Coulomb interactions, the shape of the density of states, spatial correlations of site energy, and positional disorder on transport dynamics.[3–12]

Microscopic approaches, which combine quantum chemistry, charge transfer theories, as well as molecular and statistical mechanics,[13–18] are conceptually similar to GDM, except now charge hopping sites are extracted from a large-scale morphology obtained using molecular dynamics and charge transfer rates are determined using first-principles calculations. Such a multiscale methodology allows one to directly link macroscopic observables to the chemical structure and the morphology and has been used, e.g., to elucidate the influence of stacking motifs in columnar mesophases of liquid crystals[2,19–21] and to study percolating networks and polarization effects in organic crystals.[19,22]

There exist, however, experimentally viable situations, where neither of these two approaches is suitable. The complexity of the microscopic approach limits its practical application to comparatively small system sizes, limiting simulations of transport in realistic device geometries, i.e., without periodic boundary conditions. It also does not allow one to study a relaxation of a "hot" carrier in a density of states with large energetic disorder, due to an insufficient number of available states.[23] GDM, apart from relying on experimental input, cannot properly handle interfaces and host/guest systems, due to the use of regular lattices. To tackle such problems, it would be desirable to marry the two approaches, that is, to generalize the GDM to realistic (off-lattice) morphologies and then fit the ingredients of this, generalized, model to the (calculated) properties of representative microscopic systems.

In this paper we demonstrate how this can be achieved by using stochastic models.[24,25]

As a prototypical system, we use tris-(8-hydroxyquinoline)aluminum (Alq_3), a green light emitter employed in early realizations of organic light emitting diodes.[26–34] The coordination of three organic ligands to the central aluminum atom leads to a roughly spherically shaped molecule that is known to form an amorphous phase which conducts both holes and electrons. In this disordered phase, the large molecular dipole moment results in a broad distribution of the density of states and long-range correlations of site energies.[17] Using Alq_3 as a test system for the development of a stochastic model is a considerable challenge since one has to accurately account for the significant impact of a complex energy landscape on the charge-transport properties of the material. If successful, the same procedures can be expected to perform with at least equal accuracy for less disordered materials.

To incorporate the molecular properties into the stochastic model we first perform microscopic simulations of hole transport in a small (compared to, e.g., typical device sizes, but large from the point of view of computational cost) amorphous system of Alq_3. These simulations provide the reference weighted graph, where the vertex structure and weighted edges are determined from the realistic morphology and the microscopic hopping rates, respectively. We then develop a stochastic network model, which includes generation of the dense spatial vertex structure using an iterative dominance-competition point-process model,[35] a Bernoulli model to obtain the vertex connectivity, a moving-average procedure to assign correlated site energies to vertices, and distance-dependent normal distributions to obtain electronic coupling elements. We finally validate the model by comparing field dependencies of charge carrier mobility as predicted by the stochastic and microscopic approaches.

II. MICROSCOPIC SIMULATIONS

Here, we briefly summarize the determination of the reference weighted graph obtained by microscopic simulations. For a full account of the procedure, see Ref. 17.

The first step is the generation of an amorphous morphology by atomistic molecular dynamics (MD) simulations. The force field details can be found in the supporting information of Ref. 17. A cubic box with $N = 4096$ Alq$_3$ molecules arranged on a cubic lattice is equilibrated above the glass transition temperature, at 700 K, in an NPT ensemble with a velocity rescaling thermostat and the Berendsen barostat. The system is then quenched to room temperature. All simulations are performed using the GROMACS package.[36]

The centers of mass of the molecules for a given snapshot define the hopping sites for the charge carrier or, in other words, the vertices of the directed graph. A pair of molecules is added to the list of neighbors if the distance between centers of mass of any of the three 8-hydroxyquinoline ligands is below a cutoff of 0.8 nm. For the pairs in this neighbor list, charge hopping rates are evaluated using the high temperature limit of classical charge transfer theory[37]

$$\omega_{ij} = \frac{2\pi}{\hbar} \frac{J_{ij}^2}{\sqrt{4\pi \lambda_{ij} k_B T}} \exp\left[-\frac{(\Delta \mathcal{E}_{ij} - \lambda_{ij})^2}{4\lambda_{ij} k_B T} \right], \quad (1)$$

where T is the temperature, $\hbar$ is the reduced Planck constant, and k_B is Boltzmann's constant. The pair-specific quantities are the reorganization energy λ_{ij}, the electronic coupling element, or transfer integral J_{ij}, and the driving force, $\Delta \mathcal{E}_{ij} = \Delta \mathcal{E}_{ij}^{el} + \Delta \mathcal{E}_{ij}^{ext}$, consisting of the difference in electrostatic site energies, $\Delta \mathcal{E}_{ij}^{el} = \mathcal{E}_i - \mathcal{E}_j$, and the influence of an externally applied electric field $\vec{F}$, $\Delta \mathcal{E}_{ij}^{ext} = q\vec{F}(\vec{x}_i - \vec{x}_j)$. Here q and $\vec{x}_i$ are the charge of the carrier and the position of site i. These ingredients can be determined using electronic structure techniques, classical simulation methods, or their combination.[14,17,38]

The reorganization energy was computed using density-functional theory [DFT; B3LYP functional and a 6-311G(d,p) basis set] resulting in a value of 0.23 eV which was used for all pairs of molecules. Electronic coupling elements J_{ij} were calculated for each molecular pair using DFT [Perdew-Burke-Ernzerhof functional and a triple-ζ basis set] within the dimer-projection method.[39,40] Electrostatic contributions to the site energies $\mathcal{E}_i$ are evaluated self-consistently based on the Thole model[41] with atomic partial charges and polarizabilities as in Ref. 17.

With all the ingredients at hand, rates ω_{ij} between pairs of molecules in the neighbor list are computed using Eq. (1) for $T = 290$ K. These rates define the edge weights of the reference directed graph.

III. STOCHASTIC NETWORK MODEL

We interpret the rates and the directed graph of the microscopic model as a realization of a stochastic network model with spatially distributed vertices and weighted edges. A weighted graph G can be described by the triple $G = (V, E, \Omega)$, where V is the set of vertices, E is the set of edges, and Ω is the set of edge weights. The set of vertices $V = \{S_1, S_2, \ldots\}$, where S_i is the location of the ith vertex in $\mathbb{R}^3$, describes the locations (coordinates) of the hopping sites. The set of edges $E = \{(S_{i_1}, S_{j_1}), (S_{i_2}, S_{j_2}), \ldots\}$ describes the line segments between two connected vertices, i.e., it indicates which hopping sites are connected. Finally, the set of weights

$\Omega = \{(\omega_{ij}, \omega_{ji}), (S_i, S_j) \in E\}$, where ω_{ij} is the edge weight from S_i to S_j, describes the hopping rates between hopping sites.

Note that the stochastic network model is realized in a cubic box $W = [0, w_1] \times [0, w_2] \times [0, w_3] \subset \mathbb{R}^3$, $w_1, w_2, w_3 > 0$, with periodic boundary conditions, whereby edges can be connected over matching faces of the box W, to match the setup of the microscopic simulation.

In the following, we develop and parametrize a stochastic model for the weighted graph G consisting of separate modeling components for its vertex set V, the edge set E, as well as the set of edge weights Ω.

A. Vertex set

When identifying an appropriate procedure to generate a set of points V in space with specific properties (density, correlations, etc.), i.e., a suitable point-process model, some general physical features have to be considered. First, due to the fact that the points represent the centers of mass of molecules which have finite extent, they need to have a minimum separation between them. Second, neighbor separations fluctuate, e.g., due to intercalations. Finally, systems in glassy states have a high number density $\rho = N_{mol}/w$, where N_{mol} is the number of molecules in volume $w = |W| = w_1 w_2 w_3$. Therefore, the goal is to develop a point-process model which provides both large minimum separations and high number densities.

To achieve this, we extend the existing dominance-competition point-process model,[35] which relies on the thinning of a Poisson process, depicted in Fig. 1(a). In a first step, points are generated according to a homogeneous Poisson process, that is, a number of points $N \sim \mathrm{Poi}(\rho w)$ are independently and uniformly distributed in the box W.[42] Such a process is completely random in space since points do not interact and can therefore have very short distances. To account for the finite spatial extent of the molecules, interactions are introduced by independently assigning a random radius R_n defining a spherical volume $B(S_n, R_n)$ to each point S_n, following a distribution that takes the desired nearest-neighbor distribution into account [panel (2) of Fig. 1]. Then, the point S_n is removed if it is contained in the volume of another point S_i and the volume of that point $B(S_i, R_i)$ is larger than $B(S_n, R_n)$. Such points are marked red in Fig. 1, panel (3). The set of remaining points [see panel (4) of Fig. 1] is called a dominance-competition process. In a dominance-competition process, every point S_n with radius R_n has a distance to its nearest neighboring point greater or equal than R_n. However, the maximum point density (i.e., average number of points per volume unit) of this dominance-competition model is limited[43] and eventually lower than in the microscopic model, where $\rho = 1.65$ nm^{-3}. The main issue is that the dominance-competition model is based on a thinning of a Poisson process, which has no interaction of points. Thus, the dominance-competition model cannot reproduce the short-range order observed for the vertices generated by the microscopic model.

To remedy this situation, we propose an *iterative* point-process model. Starting from the dominance-competition point pattern, Fig. 1, panel (4), a second independent realization of a dominance-competition process is generated in the empty space, as indicated by the blue circles in panel (5) of Fig. 1.
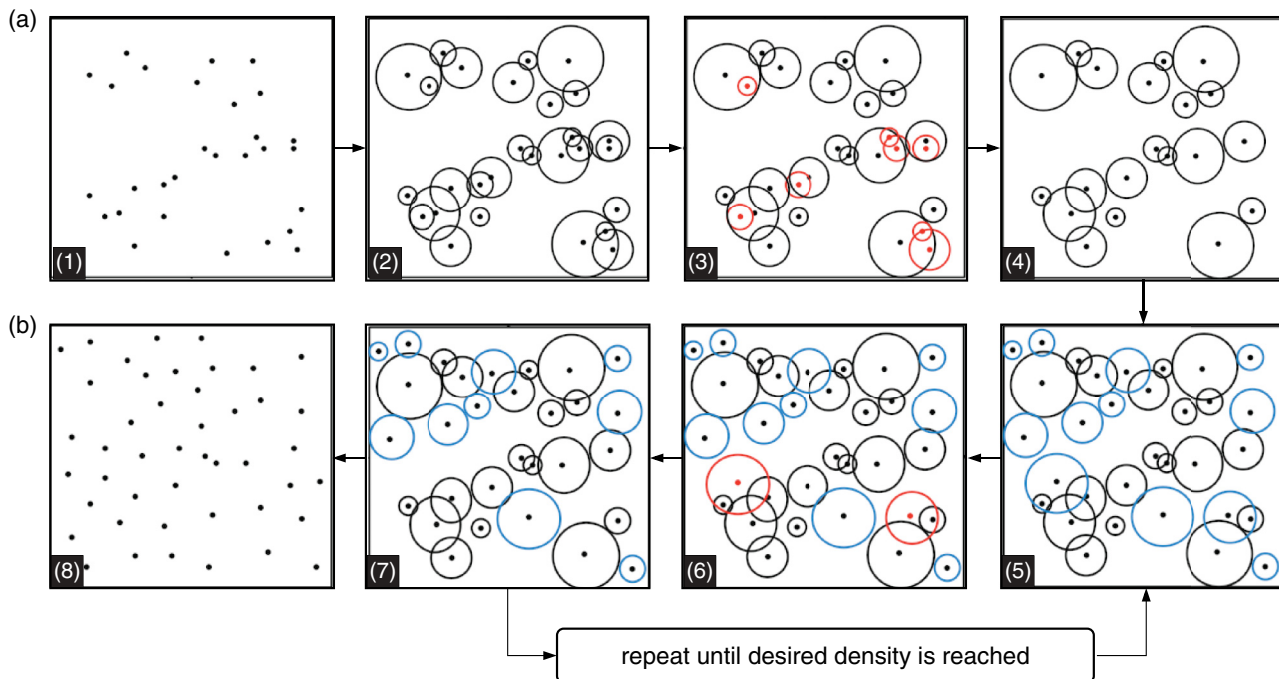
FIG. 1. (Color online) Schematic representation of the iterative dominance-competition model: (a) thinning of homogeneous Poisson process according to the dominance-competition model; and (b) iterative addition of points in the complementary phase to achieve desired point density.

Points whose volumes contain points of previous realizations [see red circles in Fig. 1, panel (6)], are deleted [panel (7) of Fig. 1]. By this, it is guaranteed that for each accepted point S_n, the distance to the nearest neighbor is always larger than R_n. These steps are repeated k times until a point pattern with the desired intensity is reached. In practice, the densities of the first $k-1$ iterations are chosen as large as possible and the density of the kth iteration is chosen such that the microscopic reference density ρ is reached.

The nearest-neighbor-distance distribution function $D(r)$, defined as the probability of a randomly chosen point to have its nearest neighboring point within a distance of $r > 0$,[35] is shown in Fig. 2(a). In the microscopic model, the hopping sites have a minimum separation of $r_h = 0.545$ nm, hence

$D(r) = 0$ for $r \leqslant r_h$. The point pattern of hopping sites is also rather regular since the nearest-neighbor distances vary only in a small range of $0.545 \leqslant r \leqslant 0.88$ nm. Therefore, the random radii R_n, which control the distances between points, are simulated according to $R_n = r_h + X_n$, where $X_1, X_2, \ldots$ are independent and identically Γ-distributed random variables with mean 0.08 nm and variance 0.002 nm^2. After $k = 7$ iterations the density $\rho = 1.65$ nm^{-3} of the microscopic data is reached.

For validation of the model, structural characteristics of the point pattern are compared to those of the microscopic model. Among these are the nearest-neighbor-distance distribution function [Fig. 2(a)], the pair-correlation function $g(r)$ [Fig. 2(b)], and the distribution function of spherical contact
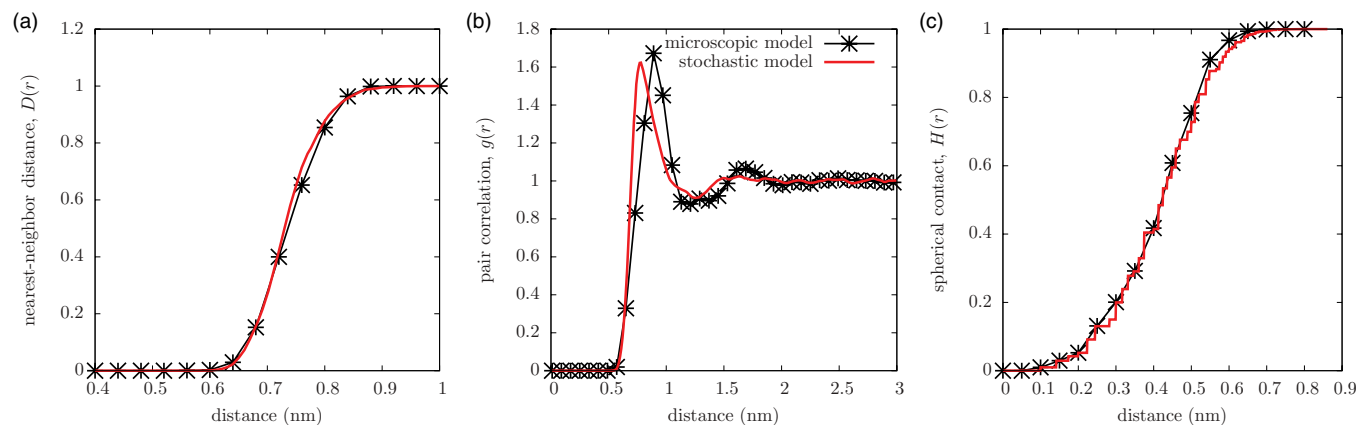

FIG. 2. (Color online) Characteristic distribution functions of the microscopic and stochastic point-process model: (a) nearest-neighbor distance distribution function; (b) pair correlation function; and (c) spherical contact distribution function.

distances $H(r)$, which is the probability that the distance from a randomly chosen point in space to the nearest point of the point pattern is smaller than r [Fig. 2(c)]. For all distributions there is a reasonable agreement between the microscopic and stochastic models.

B. Site energies

We now develop a model for the site energies $\mathcal{E}_n$. Statistically, they follow a normal distribution with mean m and variance σ^2, i.e., $\mathcal{E}_n \sim \mathcal{N}(m, \sigma^2)$. Since $\mathcal{E}_n$ are due to long-range electrostatic interactions of a localized charge with the local electric field of the surrounding neutral molecules, they are correlated in space.

To introduce spatial correlations, we propose a moving-average procedure.[44] This procedure relies on invariance properties of the normal distribution with respect to convolution, i.e., $\sum_{i=1}^{\ell} X_i \sim \mathcal{N}(\sum_{i=1}^{\ell} m_i, \sum_{i=1}^{\ell} \sigma_i^2)$, where $X_i \sim \mathcal{N}(m_i, \sigma_i^2)$ are independent random variables. Let $M_n^{(a)}, M_n^{(b)}, M_n^{(c)} \sim \mathcal{N}(0, \sigma^2)$ be three sequences of independent and identically distributed random variables. Every vertex S_n is assigned the 4$-$tuple $(S_n, M_n^{(a)}, M_n^{(b)}, M_n^{(c)})$, to which we want to allocate a random site energy $\mathcal{E}_n$. If $S_n^{(1)}, S_n^{(2)}, \ldots, S_n^{(\ell)}$ are its ℓ nearest neighbors (including the point S_n itself), with corresponding random variables $M_n^{(b),(i)}, M_n^{(c),(i)}, i = 1, \ldots, \ell$, the site energy is evaluated as

$$\mathcal{E}_n = \sqrt{\omega_a} M_n^{(a)} + \sqrt{\frac{\omega_b}{\ell_b}} \sum_{i=1}^{\ell_b} M_n^{(b),(i)}$$
$$+ \sqrt{\frac{1 - \omega_a - \omega_b}{\ell_c}} \sum_{i=1}^{\ell_c} M_n^{(c),(i)} + m,$$

where $\omega_a, \omega_b \geqslant 0 \, (\omega_a + \omega_b \leqslant 1)$ are weights for the individual components and $\ell_b, \ell_c > 0$ for some integers. The idea is to develop the energy landscape as a superposition of three independent energy landscapes with different properties. The first component, $M_n^{(a)}$, is independent, i.e., it represents a rough energy landscape. Its weight ω_a controls the magnitude of the maximum spatial correlation.

The next two components, $\sum_{i=1}^{\ell_b} M_n^{(b),(i)}$ and $\sum_{i=1}^{\ell_c} M_n^{(c),(i)}$, are strongly correlated to that of the neighboring vertices, whereas the number of nearest neighbors ℓ_b and ℓ_c controls their range of spatial distribution. The correlation function of site energies (see Fig. 3) exhibits a strong decrease for small distances as well as small correlations for long distances. To include both characteristics, we chose $\ell_b < \ell_c$, such that $\sum_{i=1}^{\ell_b} M_n^{(b),(i)}$ describes the strong decrease for small distances and $\sum_{i=1}^{\ell_c} M_n^{(c),(i)}$ describes the long-distance correlations. The parameters ω_a, ω_b, ℓ_b, ℓ_c are estimated by minimizing the discrepancy between microscopic and stochastic-model correlation functions, $\kappa(r)$.

For Alq$_3$, the site-energy distribution of the microscopic model is characterized by a mean of $m = -0.76$ eV and variance of $\sigma^2 = 0.036$ eV^2. Due to the high molecular dipole moment of a single molecule of $\sim$4 D, the energy correlation function for the microscopic model, shown in Fig. 3, has a long-range tail. The correlation function of the stochastic network model for $\omega_a = 0.2$, $\omega_b = 0.4$, $\ell_b = 9$, and $\ell_c = 280$ reproduces these correlations.
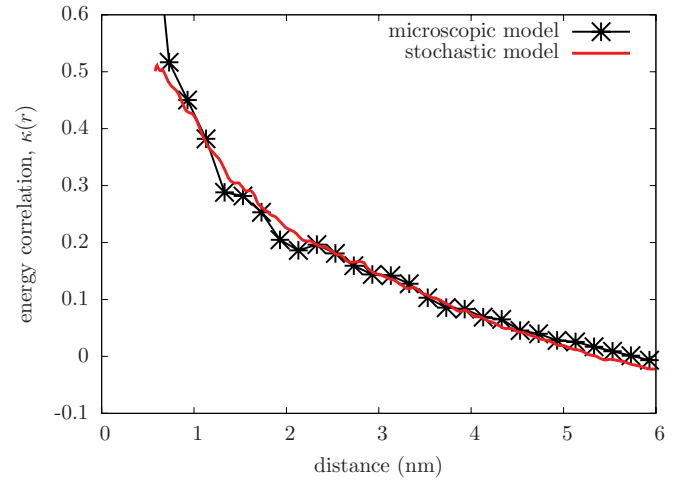

FIG. 3. (Color online) Correlation function for the site energies estimated from the microscopic model and the fitted stochastic model.

C. Graph edges

The random edge set $E = \{(S_{i_1}, S_{j_1}), (S_{i_2}, S_{j_2}), \ldots\}$ describes those pairs of vertices which are connected. Since charge transfer can only occur between the neighboring molecules, an edge set (neighbor list) of the microscopic model is based on a cutoff distance between subunits of individual molecules (ligands of Alq$_3$). Contrarily, the stochastic model operates on the molecular centers of mass (set of vertices). Thus, the procedure for the edge set generation can only rely on the information about this set.

In the microscopic model, the probability of two hopping sites being connected, $f(r)$, is unity for distances up to 1 nm and then decreases practically linearly until it is zero [see Fig. 4(a)]. In the range 0.99 nm $< r <$ 1.39 nm, a fit of the linear function yields $f(r) = -2.553r + 3.509$ (where r is in nanometers) and two vertices of the stochastic model with separation r are added to the set of edges with a probability $f(r)$.

This connectivity model is validated by analyzing the distribution of coordination numbers (the number of edges emanating from a vertex) and edge lengths. These distributions, shown in Figs. 4(b) and 4(c), are in a good agreement between the graphs generated by the microscopic and stochastic models.

D. Transfer integrals

The final component of the stochastic network model is the squared transfer integral J_{ij}^2. Microscopically, J_{ij} is determined from the electron densities of the involved molecules and their interactions on a quantum-mechanical level. As such, transfer integrals depend sensitively on the molecular electronic structure and on mutual positions and orientations of the molecules.

For Alq$_3$, analysis of the microscopic J_{ij}^2 shows that, for a fixed distance r between hoping sites, $\log_{10}(J_{ij}^2/eV^2)$ is normally distributed according to $\mathcal{N}(m(r), \sigma^2(r))$. We therefore compute the distance-dependent mean value and the variance of $\log_{10}(J_{ij}^2/eV^2)$, which is shown in Figs. 5(a) and 5(b). The mean decreases linearly with distance, which is expected from
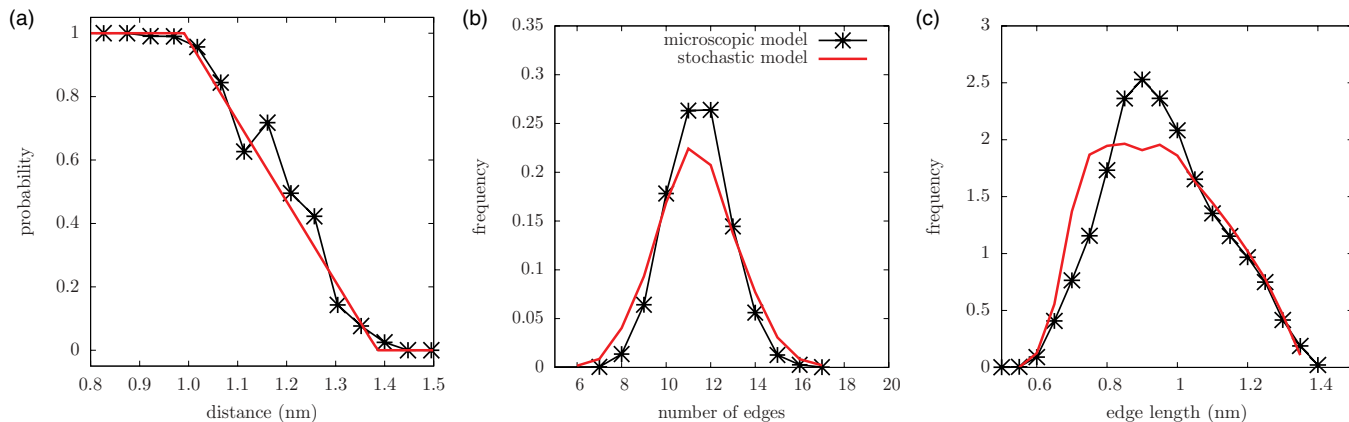
FIG. 4. (Color online) (a) Distance-dependent probability of two hopping sites being connected. Histograms of (b) coordination number and (c) edge lengths. The mean (variance) of the coordination number is 11.43 (2.03) in the microscopic model compared to 11.37 (3.18) in the stochastic model. For the edge lengths, we obtain 0.99 nm (0.03 nm^2) and 0.97 nm (0.03 nm^2), respectively.

the exponentially decaying overlap of the involved electron densities. We fit two linear curves $m(r) = -4.272r - 1.594$ and $\sigma^2(r) = 7.819r - 2.027$ to the data (r in nm, m in eV, and σ^2 in eV^2), which are also shown in Fig. 5. In the stochastic model, an edge (S_i, S_j) is assigned a squared transfer integral $J_{ij}^2 = 10^{X_{ij}}$ eV^2, where $X_{ij} \sim \mathcal{N}(m(r), \sigma^2(r))$.

IV. MODEL VALIDATION

To begin with, we compare the rate distributions predicted by the stochastic model and the reference microscopic model. In both cases the external field is set to zero, i.e., $F = 0$, where $F = |\vec{F}|$. Figure 5(c) shows that both distributions are in excellent agreement with each other.

To further validate the model, we evaluate charge mobility μ, defined as the ratio of charge velocity v over F, i.e., $\mu = v/F$. The charge velocity is determined using the kinetic Monte Carlo (KMC) algorithm by dividing the charge displacement vector along the field direction (accounting for periodic boundary conditions) by the total simulation time. To improve the statistics, the value of mobility is averaged over six different directions of the external field and several KMC trajectories starting from different injection points.

We first ignore the site-energy disorder, i.e., we put $\Delta \mathcal{E}_{ij}^{\text{el}} = 0$ in the expression for the rates in Eq. (1). The mobilities vs field (KMC simulation time 10^{-5} s, averaged over six field directions and five injection points) are shown in Fig. 6(a) for both microscopic and stochastic models. One can see that the absolute values and a slight decrease with the increasing field strength (inverted regime) are similar for both models.

Taking the energetic disorder into account reduces the value of mobility [Fig. 6(b), KMC simulation time 0.1 s, same averages as before] by six (at low fields) to five (at high fields) orders of magnitude and is due to large disorder in site energies. Here the agreement between absolute values is not perfect (there is approximately a factor of 5 difference). The disagreement is in fact not a shortcoming of the stochastic model, but is due to finite-size effects. Since the analyzed systems have a relatively small number N of sites (4096 in this work) and the corresponding site energies are strongly correlated, the distributions of site energies predicted by both the stochastic and microscopic models have significant fluctuations from one realization to another, especially in systems with large energetic disorder. The simplest way of illustrating this is by calculating the average energy of a charge in equilibrium, $\bar{\mathcal{E}}$. Assuming that the system is ergodic and the
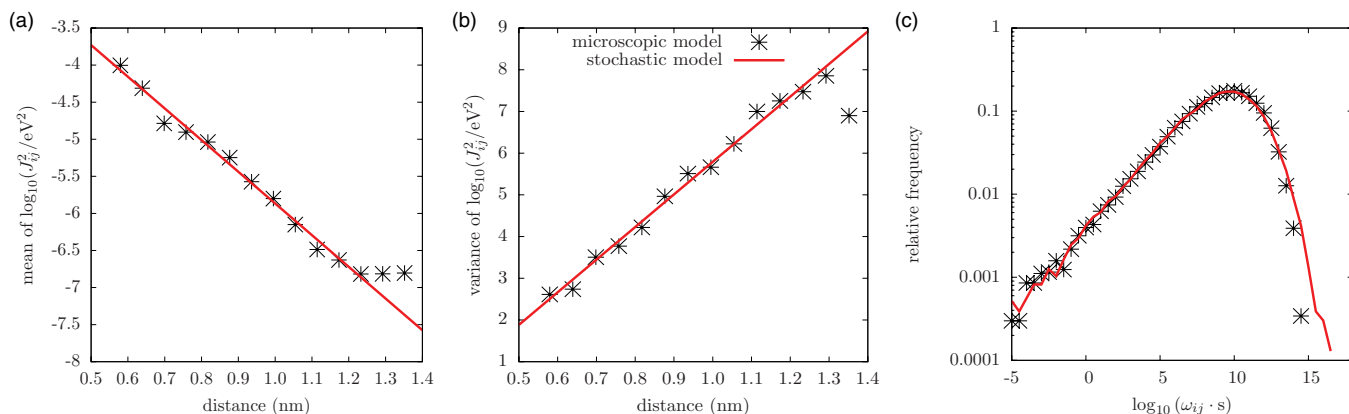

FIG. 5. (Color online) Mean (a) and variance (b) of distributions of $\log_{10}(J_{ij}^2/\text{eV}^2)$ as a function of distance between hopping sites. (c) Distributions of logarithmic transfer rates $\log_{10}(\omega_{ij}\text{s})$.
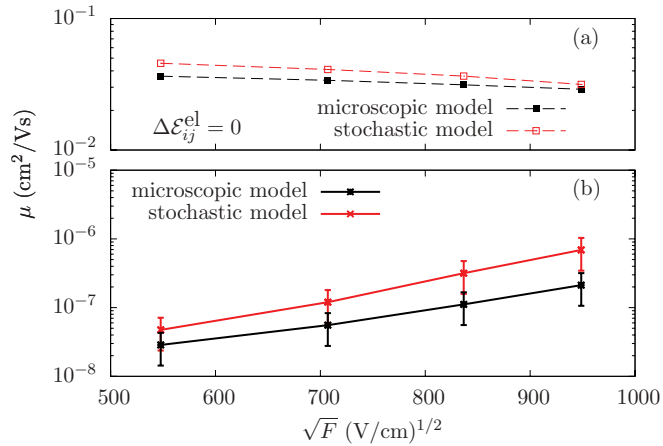
FIG. 6. (Color online) Hole mobilities μ as a function of applied field F, based on the microscopic (black) and stochastic (red) graph. (a) Results obtained without site-energy disorder, i.e., $\Delta \mathcal{E}_{ij}^{el} = 0$. (b) Poole-Frenkel plot. Error bars for the stochastic model have been determined by averaging over three independent realizations. Since respective errors cannot be calculated for the microscopic model due to the computational cost of generating and evaluating independent snapshots, relative errors identical to the stochastic model have been assumed.

occupation probabilities are Boltzmann-distributed, $\bar{\mathcal{E}}$ reads

$$\bar{\mathcal{E}} = \sum_{n=1}^{N} \mathcal{E}_n \exp(-\mathcal{E}_n / k_B T) \Big/ \sum_{n=1}^{N} \exp(-\mathcal{E}_n / k_B T). \quad (2)$$

For the realizations of the stochastic model used for averaging, we find $\bar{\mathcal{E}}/k_B T = (-25.09, -23.65, -28.21)$ relative to the mean m of the distribution, while for the microscopic model $\bar{\mathcal{E}}/k_B T = -26.01$. Higher average energies lead to significantly higher mobilities and, as discussed in Ref. 23, pronounced finite-size effects (higher mobilities) when *mobilities* are averaged over several realizations of site-energy distributions. To partially remedy the situation, one could either prefilter realizations of the stochastic model to those with the same transport level or increase the size of the microscopic reference. However, even doubling of the microscopic reference size is computationally prohibitive at the level of theory we employed in our calculations (DFT-based evaluation of coupling elements, self-consistent polarization model for site energies). Moreover, finite-size effects become negligibly small only if $(\sigma/k_B T)^2 \lesssim -5.7 + 1.05 \ln N$, in our case for $N \approx 10^{26}$ (see, again, Ref. 23). So even for a perfect

parametrization of the stochastic model, one has to expect systematic finite-size effects and concomitant deviations between microscopic and stochastic models.[45] Given the high sensitivity of mobilities to the finite-size effects and the fact that according to the rate expression, Eq. (1), deviations in the parametrization propagate exponentially into the mobility, the achieved agreement is satisfying: Both models predict that, as a result of strongly correlated energetic disorder, mobility is reduced by six orders of magnitude as compared to the (hypothetical) disorder-free case. Similarly, the mobility increase with the strength of the field F, $\mu \sim \exp(\alpha \sqrt{F})$, which is again due to correlated site-energy disorder, and the slope of this dependence, α, also known as a Poole-Frenkel slope, is well reproduced. Overall, the stochastic model captures the relevant physics of charge transport as characterized by the field-dependent mobility on a qualitative and quantitative level, even though the parametrization of the model did not explicitly use μ as a target property, but instead the details of the underlying graph representation of the charge transport network. The computational cost of creating this weighted graph is on the order of seconds for the stochastic model as compared to weeks for the microscopic description. The stochastic model is therefore transferable to situations whose treatment is beyond the computational limits of microscopic simulations of charge transport.

V. SUMMARY

To summarize, we have developed a stochastic network model of the directed weighted graph used for microscopic charge transport simulations. The model, parametrized for a prototypical amorphous organic semiconductor, tris-(8-hydroxyquinoline)aluminum, showed good agreement with the predictions of the microscopic approach: Both the mobility-field dependence and distributions of the charge transfer rates were adequately reproduced. The generalization of the model to more complex situations, e.g., anisotropic in shape molecules and molecular mixtures, is possible and is a work in progress.

*baumeier@mpip-mainz.mpg.de

[1] Y. Shirota and H. Kageyama, Chem. Rev. **107**, 953 (2007).

[2] X. L. Feng, V. Marcon, W. Pisula, M. R. Hansen, J. Kirkpatrick, F. Grozema, D. Andrienko, K. Kremer, and K. Müllen, Nature Mater. **8**, 421 (2009).

[3] P. M. Borsenberger, L. Pautmeier, and H. Bässler, J. Chem. Phys. **94**, 5447 (1991).

[4] H. Bässler, Phys. Status Solidi B **175**, 15 (1993).

[5] S. V. Novikov, D. H. Dunlap, V. M. Kenkre, P. E. Parris, and A. V. Vannikov, Phys. Rev. Lett. **81**, 4472 (1998).

[6] A. B. Walker, A. Kambili, and S. J. Martin, J. Phys.: Condens. Matter. **14**, 9825 (2002).

[7] W. F. Pasveer, J. Cottaar, C. Tanase, R. Coehoorn, P. A. Bobbert, P. W. M. Blom, D. M. de Leeuw, and M. A. J. Michels, Phys. Rev. Lett. **94**, 206601 (2005).

[8] Y. Yimer, P. Bobbert, and R. Coehoorn, Synth. Met. **159**, 2399 (2009).

[9] M. Bouhassoune, S. v. Mensfoort, P. Bobbert, and R. Coehoorn, Org. Electron. **10**, 437 (2009).

[10] J. A. Freire and C. Tonezer, J. Chem. Phys. **130**, 134901 (2009).

[11] J. Cottaar, L. J. A. Koster, R. Coehoorn, and P. A. Bobbert, Phys. Rev. Lett. **107**, 136601 (2011).

[12] J. J. M. van der Holst, F. W. A. van Oost, R. Coehoorn, and P. A. Bobbert, Phys. Rev. B **83**, 085206 (2011).

[13] J. Kirkpatrick, V. Marcon, J. Nelson, K. Kremer, and D. Andrienko, Phys. Rev. Lett. **98**, 227402 (2007).

[14] V. Coropceanu, J. Cornil, D. A. da Silva Filho, Y. Olivier, R. Silbey, and J. Brédas, Chem. Rev. **107**, 926 (2007).

[15] D. Andrienko, J. Kirkpatrick, V. Marcon, J. Nelson, and K. Kremer, Phys. Status Solidi B **245**, 830 (2008).

[16] J. Nelson, J. J. Kwiatkowski, J. Kirkpatrick, and J. M. Frost, Acc. Chem. Res. **42**, 1768 (2009).

[17] V. Rühle, A. Lukyanov, F. May, M. Schrader, T. Vehoff, J. Kirkpatrick, B. Baumeier, and D. Andrienko, J. Chem. Theory Comput. **7**, 3335 (2011).

[18] B. Baumeier, F. May, C. Lennartz, and D. Andrienko, J. Mater. Chem. **22**, 10971 (2012).

[19] T. Vehoff, B. Baumeier, and D. Andrienko, J. Chem. Phys. **133**, 134901 (2010).

[20] T. Vehoff, B. Baumeier, A. Troisi, and D. Andrienko, J. Am. Chem. Soc. **132**, 11702 (2010).

[21] F. May, V. Marcon, M. R. Hansen, F. Grozema, and D. Andrienko, J. Mater. Chem. **21**, 9538 (2011).

[22] M. Schrader, R. Fitzner, M. Hein, C. Elschner, B. Baumeier, K. Leo, M. Riede, P. Bäuerle, and D. Andrienko, J. Am. Chem. Soc. **134**, 6052 (2012).

[23] A. Lukyanov and D. Andrienko, Phys. Rev. B **82**, 193202 (2010).

[24] O. Stenzel, H. Hassfeld, R. Thiedmann, L. J. A. Koster, S. D. Oosterhout, S. S. van Bavel, M. M. Wienk, J. Loos, R. A. J. Janssen, and V. Schmidt, Ann. Appl. Stat. **5**, 1920 (2011).

[25] O. Stenzel, L. J. A. Koster, R. Thiedmann, S. D. Oosterhout, R. A. J. Janssen, and V. Schmidt, Adv. Funct. Mater. **22**, 1236 (2012).

[26] D. Z. Garbuzov, V. Bulovic, P. E. Burrows, and S. R. Forrest, Chem. Phys. Lett. **249**, 433 (1996).

[27] R. L. Martin, J. D. Kress, I. H. Campbell, and D. L. Smith, Phys. Rev. B **61**, 15804 (2000).

[28] A. Djurisic, C. Kwong, T. Lau, E. Li, Z. Liu, H. Kwok, L. Lam, and W. Chan, Appl. Phys. A. **76**, 219 (2003).

[29] M. Cölle and W. Brütting, Phys. Status Solidi A **201**, 1095 (2004).

[30] H. H. Fong and S. K. So, J. Appl. Phys. **100**, 094502 (2006).

[31] W. Brütting, *Physics of Organic Semiconductors*, 1st ed. (Wiley-VCH, Weinheim, 2005).

[32] M. Knupfer, Appl. Phys. A. **94**, 31 (2008).

[33] J. J. Kwiatkowski, J. Nelson, H. Li, J. L. Brédas, W. Wenzel, and C. Lennartz, Phys. Chem. Chem. Phys. **10**, 1852 (2008).

[34] Y. Nagata and C. Lennartz, J. Chem. Phys. **129**, 034709 (2008).

[35] J. Illian, A. Penttinen, H. Stoyan, and D. Stoyan, *Statistical Analysis and Modeling of Spatial Point Patterns* (Wiley, Chichester, 2009).

[36] B. Hess, C. Kutzner, D. van der Spoel, and E. Lindahl, J. Chem. Theory Comput. **4**, 435 (2008).

[37] R. A. Marcus, Rev. Mod. Phys. **65**, 599 (1993).

[38] J. Brédas, D. Beljonne, V. Coropceanu, and J. Cornil, Chem. Rev. **104**, 4971 (2004).

[39] E. F. Valeev, V. Coropceanu, D. A. da Silva Filho, S. Salman, and J. Brédas, J. Am. Chem. Soc. **128**, 9882 (2006).

[40] B. Baumeier, J. Kirkpatrick, and D. Andrienko, Phys. Chem. Chem. Phys. **12**, 11103 (2010).

[41] B. Thole, Chem. Phys. **59**, 341 (1981).

[42] A Poisson-based point process holds good formal properties for infinite space, such as the definition of several point-process characteristics.

[43] A. Delarue and D. Jeulin, Image Anal. Stereol. **20**, 181 (2001).

[44] R. Thiedmann, I. Manke, W. Lehnert, and V. Schmidt, J. Mater. Sci. **46**, 7745 (2011).

[45] Indeed, when employing a simpler (and less physical) macroscopic model based on a dielectric constant $\epsilon_r = 3.0$ in the calculation of site energies for the microscopic reference model, we obtain considerably lower ($\sigma^2 = 0.008$ eV) and less correlated [$\kappa(r) = 0$ for $r \geqslant 2$ nm] disorder, finite-size effects become insignificant and a respective stochastic model agrees within 5% with the microscopic model.